Chem Catalysis

CellPress
OPEN ACCESS

Article

The role of binding modules in enzymatic poly(ethylene terephthalate) hydrolysis at high-solids loadings

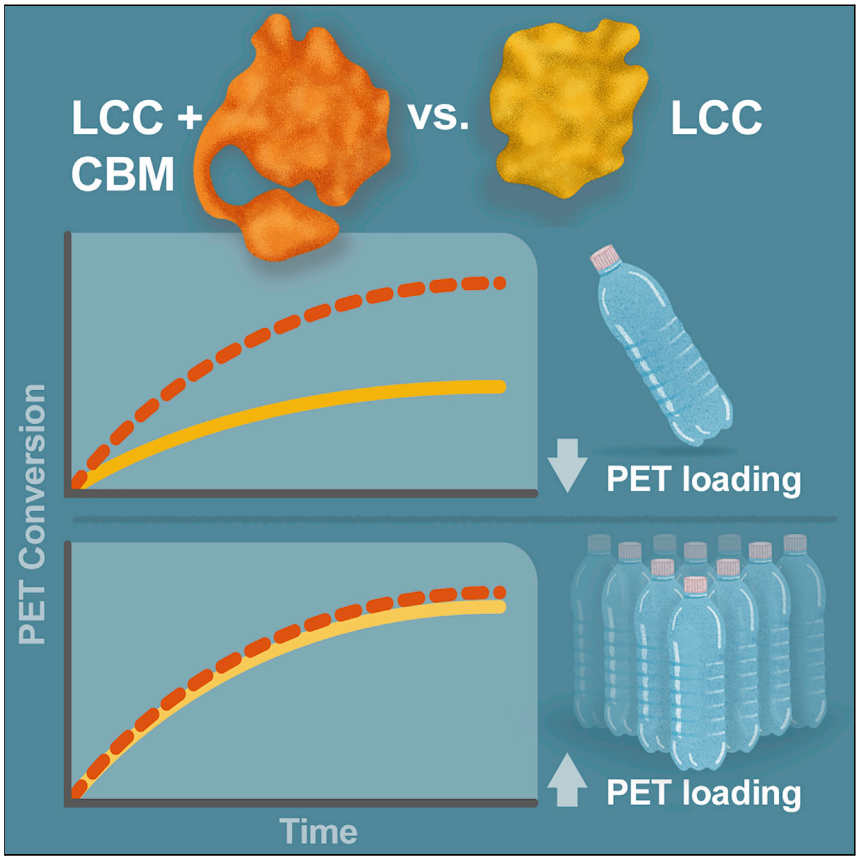

Enzymatic recycling of PET offers a promising solution to the global plastic problem. Research into accessory domains to enhance PET turnover has so far not been tested at high PET solids loadings. Here, we show that carbohydrate-binding domains do not offer any benefit at high PET solids loadings that are relevant to industrial-scale biorecycling.

Rosie Graham, Erika Erickson, Richard K. Brizendine, ..., Gregg T. Beckham, John E. McGeehan, Andrew R. Pickford

andy.pickford@port.ac.uk

Highlights

A new variant of LCC exhibits higher thermostability and greater PET turnover

Specific CBMs stimulate PET hydrolysis at low-solids loading

The advantage of these CBMs is lost at industrially relevant high-solids loading

Graham et al., Chem Catalysis *2*, 2644–2657
October 20, 2022 Published by Elsevier Inc.
https://doi.org/10.1016/j.checat.2022.07.018

CellPress
OPEN ACCESS

Chem Catalysis

Article

The role of binding modules in enzymatic poly(ethylene terephthalate) hydrolysis at high-solids loadings

Rosie Graham,[1,2] Erika Erickson,[2,3] Richard K. Brizendine,[2,3] Davinia Salvachúa,[3] William E. Michener,[2,3] Yaohao Li,[4] Zhongping Tan,[4] Gregg T. Beckham,[2,3] John E. McGeehan,[1,2] and Andrew R. Pickford[1,2,5,*]

SUMMARY

In nature, enzymes that deconstruct biological polymers, such as cellulose and chitin, often exhibit multi-domain architectures, comprising a catalytic domain and a non-catalytic binding module; the latter serves to increase the enzyme concentration at the substrate surface. This multi-domain architecture has been shown to improve the hydrolysis of poly(ethylene terephthalate) (PET) using engineered cutinase enzymes. Here, we examine the role of accessory binding modules at industrially relevant PET solids loadings necessary for cost-effective enzymatic recycling. Using a thermostable variant of leaf compost cutinase (LCC), we produced synthetic fusion constructs of LCC with five type A carbohydrate-binding modules (CBMs). At solids loadings below 10 wt %, the CBMs improve aromatic monomer yield from PET, but above this threshold, conversion extents up to 97% are reached with no added benefits from the presence of CBM fusions. This suggests that fusion constructs with the herein studied CBMs are not necessary for industrial enzymatic PET recycling.

INTRODUCTION

Poly(ethylene terephthalate) (PET) is one of the most abundantly produced single-use plastics worldwide and is used for common commercial products including food packaging, water bottles, and textiles.[1] Currently only a small fraction of post-consumer PET is recycled, and therefore the development of effective approaches to control PET pollution is of keen global interest.[2–5] This critical need has catalyzed investigation into the use of enzymes for PET deconstruction as a means of chemical recycling or upcycling.[6–12] These PET hydrolases primarily include cutinase enzymes of thermophilic origin, among other closely related biocatalysts for PET hydrolysis.[1,13,14] Enzyme engineering to attain enhanced catalytic performance and thermostability has been pursued with multiple design approaches.[15–23] Prominently, two engineered variants of the leaf-compost cutinase (LCC) (WCCG and ICCG) were reported with enhanced thermostability and have been shown to achieve up to 90% conversion of amorphous PET to monomers in less than 20 h.[22]

Beyond improvements in thermal stability, another enzyme engineering strategy that has been pursued focuses on improving enzyme binding affinity to PET.[24–29] This approach has employed multi-domain enzyme architectures comprising a catalytic domain and a non-catalytic accessory binding module, a composition commonly observed in enzyme systems that deconstruct natural biopolymers. In

THE BIGGER PICTURE

Closed-loop recycling and open-loop upcycling of waste plastics represent a suite of critical technologies to address the plastic-waste pollution crisis. Enzymatic deconstruction of the synthetic polyester poly(ethylene terephthalate) (PET) is among the several options available for chemical recycling of this common plastic. While early demonstrations of enzymatic PET recycling have shown feasibility, the technology is not yet cost competitive with production of virgin petroleum-derived PET. This study analyzes an enzyme engineering approach that takes a lesson from nature to improve the catalytic efficiency of PET-hydrolyzing enzymes and evaluates the impact of this strategy under reaction conditions that simulate a key industrial feature of enzymatic PET recycling. The implications of this study can help focus the resources available to the field on solutions that can enable rapid deployment of viable technologies to realistically address plastics pollution.

particular, this multi-domain enzyme architecture is prominently observed in enzymatic cellulose and chitin hydrolysis, wherein enzymes often contain carbohydrate-binding modules (CBMs).[30–32] Given the inherent diversity in carbohydrate structure, CBMs vary broadly in their substrate specificity and mode of binding and are classified into three types, dependent on the mechanism of substrate interaction: type A for planar binding, B for exo-binding, and C for endo-binding.[31] Of particular relevance to PET, type A CBMs bind to insoluble carbohydrates via a planar hydrophobic binding face, where the conserved aromatic residues on the binding surface align with cellulose or chitin polymer chains.[33,34] Cellulose, like PET, is hydrophobic and exhibits both crystalline and amorphous regions.[35,36] Thus, engineering CBMs, as well as other types of non-catalytic binding proteins such as hydrophobins and polyhydroxyalkanoate-binding modules, into PET hydrolases has been explored to increase the enzyme concentration on the surface of the PET substrate to enhance its hydrolysis.[24–29,37,38]

While substantial progress has been made in increasing PET deconstruction by fusion with non-catalytic binding modules in the laboratory, the goal of PET hydrolase engineering is to ultimately develop enzymes and associated processes that are industrially viable. Typically, enzymatic PET recycling involves loading a mechanically pretreated PET suspension into a stirred vessel reactor, where it is combined with enzymes for hydrolysis into the monomers terephthalic acid (TPA) and ethylene glycol (EG).[22] Recently, we reported a techno-economic analysis (TEA) of this process, highlighting the importance of high PET solids loading during hydrolysis.[39] Similar to PET, industrial cellulose hydrolysis also requires high-solids loading, typically $\geq$15 wt %, for economic viability.[40] In seminal work on cellulase engineering, Varnai et al. previously demonstrated that CBMs are not required at high-solids loading, which the authors attribute to the short diffusion path lengths required for enzymes to dissociate and access new regions of the substrate.[41,42] To date, studies that examine PET hydrolases with non-catalytic binding module fusions have only been reported for reactions with <3 wt % PET loading (Table 1), considerably below an industrially relevant level (>10 wt %).[39]

In this study, taking inspiration from Varnai et al.,[41,42] we analyze fusion enzymes of an LCC variant coupled to five different type A CBMs, characterizing their thermal stability, surface adsorption, and ability to hydrolyze PET films across a range of substrate loadings (1–20 wt %). Specifically, we evaluate the potential for utilizing CBM fusions at industrially relevant PET loadings (>10 wt %) and high conversion extents (>90%).

RESULTS

Engineered LCC-based fusion enzymes generated from five type A CBM families

Previously, Tournier et al. replaced a Ca^{2+} binding site in LCC with a disulphide bond (D238C/S283C), resulting in a more thermostable variant but at the cost of a 28% fall in PET hydrolysis activity.[22] Subsequently, this activity loss was recovered by the mutation of Phe243 to either Trp or Ile. Additionally, introducing the Y243G mutation to each enzyme gave the best-performing hydrolases against amorphized post-consumer waste PET, LCC^{WCCG} (F243W/D238C/S283C/Y127G) and LCC^{ICCG} (F243I/D238C/S283C/Y127G).[22] Here, we investigated the more conservative Phe-to-Tyr mutation at position 243, which was not reported in the previous study.[22] This new LCC variant, LCC^{YCCG} (F243Y/D238C/S283C/Y127G), has a melting transition (T_m) of 97.5°C, which is 2°C–3°C higher than the LCC^{WCCG} and LCC^{ICCG} variants (Table S1) and exhibits improved hydrolysis of PET (Figure 1A).[22] Therefore, the LCC^{YCCG} variant was adopted as the catalytic domain for CBM fusions in this study.

[1]Centre for Enzyme Innovation, School of Biological Sciences, University of Portsmouth, Portsmouth PO1 2DY, UK

[2]BOTTLE Consortium, Golden, CO 80401, USA

[3]Renewable Resources and Enabling Sciences Center, National Renewable Energy Laboratory, Golden, CO 80401, USA

[4]State Key Laboratory of Bioactive Substance and Function of Natural Medicines, Institute of Materia Medica, Chinese Academy of Medical Sciences and Peking Union Medical College, Beijing 100050, China

[5]Lead contact

*Correspondence: andy.pickford@port.ac.uk

https://doi.org/10.1016/j.checat.2022.07.018

Table 1. Studies using accessory binding modules for PET deconstruction

Enzyme catalytic domain	Accessory binding module	Accession number of accessory domain	Substrate[a]	Enzyme loading (units as reported)	Enzyme loading (mg/g PET)	PET loading (wt %)	Reference
Thc_CUT1	hydrophobin (HFB4)	XP_006964739.1	amorphous PET	5 μM	19.4	1	Ribitsch et al.[26]
Thc_CUT1	hydrophobin (HFB7)	KP209450	amorphous PET	5 μM	20.5	1	Ribitsch et al.[26]
Thc_CUT1	hydrophobin (HFB9B)	EHK16817	amorphous PET	5 μM	23.0	1	Ribitsch et al.[26]
Thc_CUT1	*Trichoderma reesei* (*Tr*CBM1)	P62694.1	amorphous PET	25 μM	28.6	3	Ribitsch et al.[25]
Thc_CUT1	polyhydroxyalkanoate depolymerase binding module (*Af*PBM)	AAA21974.1	amorphous PET	25 μM	29.1	3	Ribitsch et al.[25]
PETase	hydrophobin (RolA)	AB094496	amorphous PET	20 μM	ND	ND[b]	Puspitasari et al.[27]
PETase	*Trichoderma reesei* (*Tr*CBM1)	P62694.1	amorphous PET	10 μg/mL	1.6–6.6	0.15–0.6[c]	Dai et al.[28]
PETase	polyhydroxyalkanoate depolymerase binding module (*Af*PBM)	AAA21974.1	amorphous PET	10 μg/mL	1.6–6.6	0.15–0.6[c]	Dai et al.[28]
PETase	hydrophobin (HFB4)	XP_006964739.1	amorphous PET	10 μg/mL	1.6–6.6	0.15–0.6[c]	Dai et al.[28]
Tfuc2	dermaseptin SI (DSI)	Unknown	amorphous PET particles[d]	7 μM	23.1	1	Liu et al.[38]
LCC^{ICCG}	polyhydroxyalkanoate depolymerase binding module (*Af*PBM)	AAA21974.1	amorphous PET	0.5 μM	28.5	0.06	Xue et al.[29]
LCC^{ICCG}	*Trichoderma reesei* (*Tr*CBM1)	P62694.1	amorphous PET	0.5 μM	26.5	0.06	Xue et al.[29]
LCC^{ICCG}	hydrophobin (HFB4)	XP_006964739.1	amorphous PET	0.5 μM	32.0	0.06	Xue et al.[29]
LCC^{ICCG}	chitin binding domain (*Ch*BD)	MG210568	amorphous PET	0.5 μM	41.3	0.06	Xue et al.[29]
LCC^{YCCG}	*Trichoderma reesei* (*Tr*CBM1)	P62694.1	amorphous PET	0.05–1 μM	0.15, 1.9	1–20	this study
LCC^{YCCG}	*Thermobifida fusca* (*Tf*CBM2a)	AAD39947.1	amorphous PET	0.05–1 μM	0.18	1–20	this study
LCC^{YCCG}	*Bacillus subtilis* (*Bs*CBM3)	AAZ22322.1	amorphous PET	0.05–1 μM	0.20	1–20	this study
LCC^{YCCG}	*Teredinibacter turnerae* (*Tt*CBM10)	ABS72374.1	amorphous PET	0.05–1 μM	0.17	1–20	this study
LCC^{YCCG}	*Spirochaeta thermophila* (*St*CBM64a)	ADN02703.1	amorphous PET	0.05–1 μM	0.18	1–20	this study

[a]Sourced from Goodfellow unless stated otherwise.
[b]Parameter required for accurate determination of wt % PET loading is not described in the cited publication.
[c]Calculation based on a range as volume of vessel disclosed; however no final volume of reaction reported.
[d]Amorphous PET particles were produced using liquid nitrogen and SDS.

We selected five type A CBMs that exhibit planar surfaces for designing the fusion constructs in this study. Type A CBMs from families 1, 2a, 3, 10, and 64 were selected from both fungal and bacterial origins (Table 1).[43] These were fused to the C terminus of LCC^{YCCG} using the flexible linker from the *Trichoderma reesei* family 7 cellobiohydrolase (*Tr*Cel7A) and expressed in *Escherichia coli*.[32,44] A summary of these constructs is presented in Figure 1B, and their sequences are provided in Table S2. The *Tr*Cel7A linker is intrinsically disordered and would be glycosylated in its native host.[44–46] Expression of each LCC^{YCCG}:CBM fusion enzyme was successful, with yields ranging from 1 to 10 mg enzyme per L culture after two chromatography purification steps.

LCC^{YCCG}:CBM fusions retain esterase activity and PET binding activity

Initially, we measured the intrinsic esterase activity and PET binding activity of each LCC^{YCCG}:CBM fusion enzyme to assess any potential negative impact of the linker-CBM fusion on the catalytic domain function. Esterase activity, as measured from the hydrolysis of the diester bis(2-hydroxyethyl) terephthalate (BHET), was largely

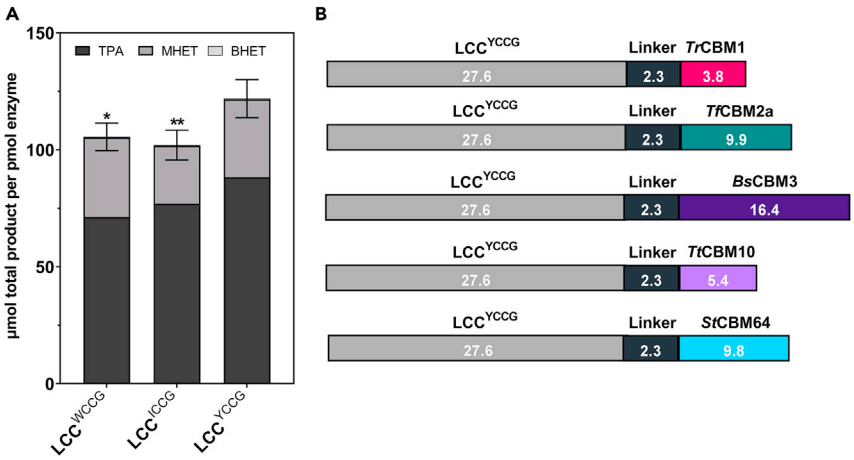

Figure 1. Design of the LCC:CBM fusion enzymes

(A) Monomeric aromatic products released following incubation for 24 h with 1 μM enzyme (1.3 mg enzyme/g PET) and PET film at 2 wt % for the three enzyme variants of LCC. Error bars represent the SD of total product from experiments performed in triplicate. Asterisks indicate statistically significant comparisons between LCC^{YCCG} and each of the other variants with *$p \leq 0.05$, and **$p \leq 0.025$.

(B) Graphical representation of the fusion enzymes generated for this study. Values represent the molecular weight (kDa) of each respective component of the construct.

Additional information is provided in Table S2 on primary sequences, family, origin, and accession number for the CBMs.

unaffected by the addition of the *Tr*Cel7A linker and any of the CBMs, with total product yields varying by ≤12.5% (Figure S1).

Langmuir isotherms of PET binding at room temperature were generated for the LCC^{YCCG} catalytic domain alone and for the five fusion enzymes using a protein concentration-based assay (Figure 2). These assays confirm that LCC^{YCCG} and all fusions bind PET and that, with the exception of LCC^{YCCG}:*Bs*CBM3, the binding capacity of the PET surface for enzyme remains unchanged irrespective of the choice of CBM. LCC^{YCCG}:*Bs*CBM3 exhibits reduced surface binding at an elevated enzyme concentration (>100 nM), suggesting that it may be prone to aggregation in solution at room temperature. The derived equilibrium dissociation constant (K_D) values for the enzymes reveal that the LCC^{YCCG}:*Tr*CBM1 fusion exhibits the highest affinity for PET (Table S3), approximately 3 times higher than that of the catalytic domain alone ($p = 0.0224$), suggesting that this CBM significantly enhances enzyme localization to the PET surface. Notably, the free energy of binding for this interaction between *Tr*CBM1 and PET (−2.80 kJ/mol), as calculated from the ratio of K_D values for LCC^{YCCG} and LCC^{YCCG}:*Tr*CBM1, is approximately half of that for binding of *Tr*CBM1 to its natural substrate, cellulose (−5.61 kJ/mol[47]).

CBMs vary in thermal stability when fused to LCC^{YCCG}

Enzyme-catalyzed PET hydrolysis is well known to be strongly temperature dependent, with contributing factors from both varying substrate properties and enzyme thermostability. Therefore, we used differential scanning calorimetry (DSC) to assess the thermostability of the component domains in each LCC^{YCCG}:CBM fusion enzyme, in addition to CBMs expressed as independent proteins (Figure 3; Table S4). For each LCC^{YCCG}:CBM fusion, a thermal unfolding transition was observed at a near-identical temperature to that for the isolated LCC^{YCCG}, confirming the minimal impact of

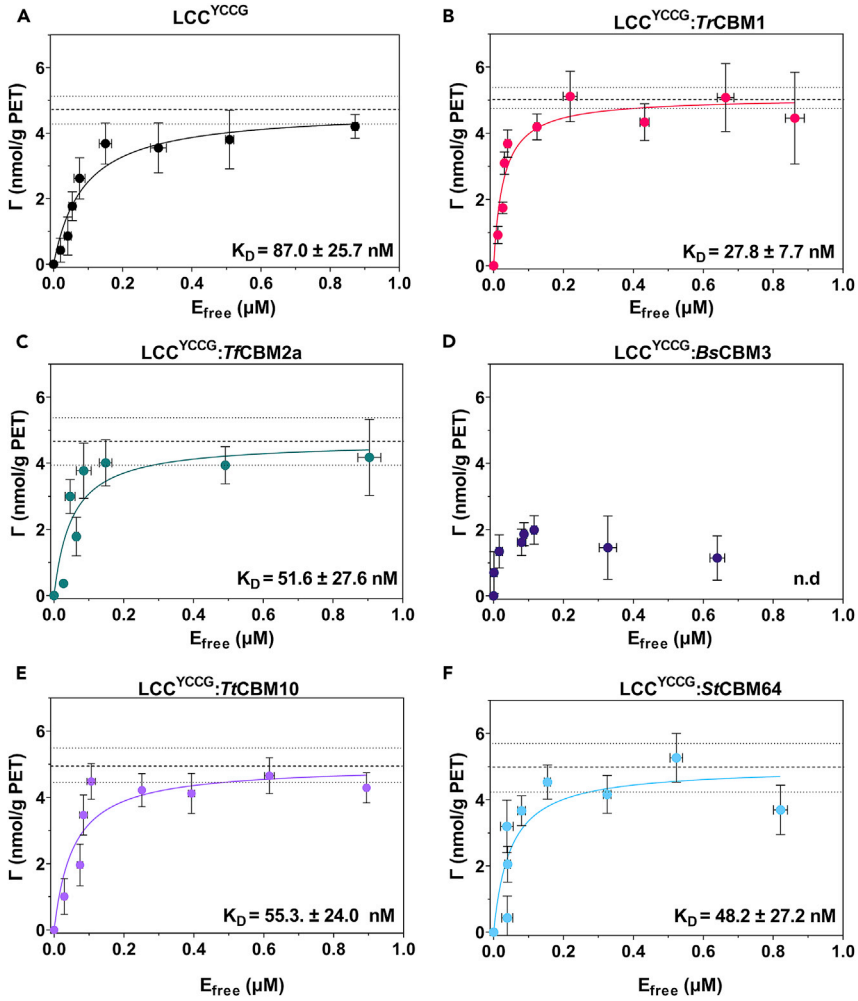

Figure 2. PET binding activity of LCC^{YCCG}:CBM fusions

(A–F) Substrate coverage as a function of free enzyme concentration used to develop Langmuir binding isotherms. Experiments were conducted at room temperature on 2 wt % amorphous PET film for LCC^{YCCG} (A), LCC^{YCCG}:*Tr*CBM1 (B), LCC^{YCCG}:*Tf*CBM2a (C), LCC^{YCCG}:*Bs*CBM3 (D), LCC^{YCCG}:*Tt*CBM10 (E), and LCC^{YCCG}:*St*CBM64 (F). Error bars represent the SD of measurements from incubations performed in triplicate. A binding threshold at the highest enzyme concentration of 2 nmol/g PET was considered significant for numerical analysis. K_D values with standard deviations are shown on each respective panel, and surface saturation (Γ_{max}) is represented with dashed lines on each graph, with dotted lines representing standard deviations.

Full binding parameters can be found in Table S3. Data are available in Data S2.

the linker-CBM fusion on the properties of the catalytic domain. For LCC^{YCCG}:*Tf*CBM2a, LCC^{YCCG}:*Bs*CBM3, and LCC^{YCCG}:*St*CBM64, discrete unfolding transitions were also observed for the CBM, albeit at a somewhat higher (for LCC^{YCCG}:*Tf*CBM2a) or lower (for LCC^{YCCG}:*Bs*CBM3 and LCC^{YCCG}:*St*CBM64) temperature than the corresponding isolated CBM. This indicates that fusion to LCC^{YCCG} can alter a CBM T_m in a CBM-dependent manner. At temperatures above the T_m of their CBM, we expect the PET hydrolysis activity of each fusion to be approximately equivalent to that of the isolated LCC^{YCCG}, although it is possible that a thermally denatured CBM might still enhance substrate binding by interacting in a non-native conformation, as seen for α-chymotrypsin adhering to Teflon.[48]

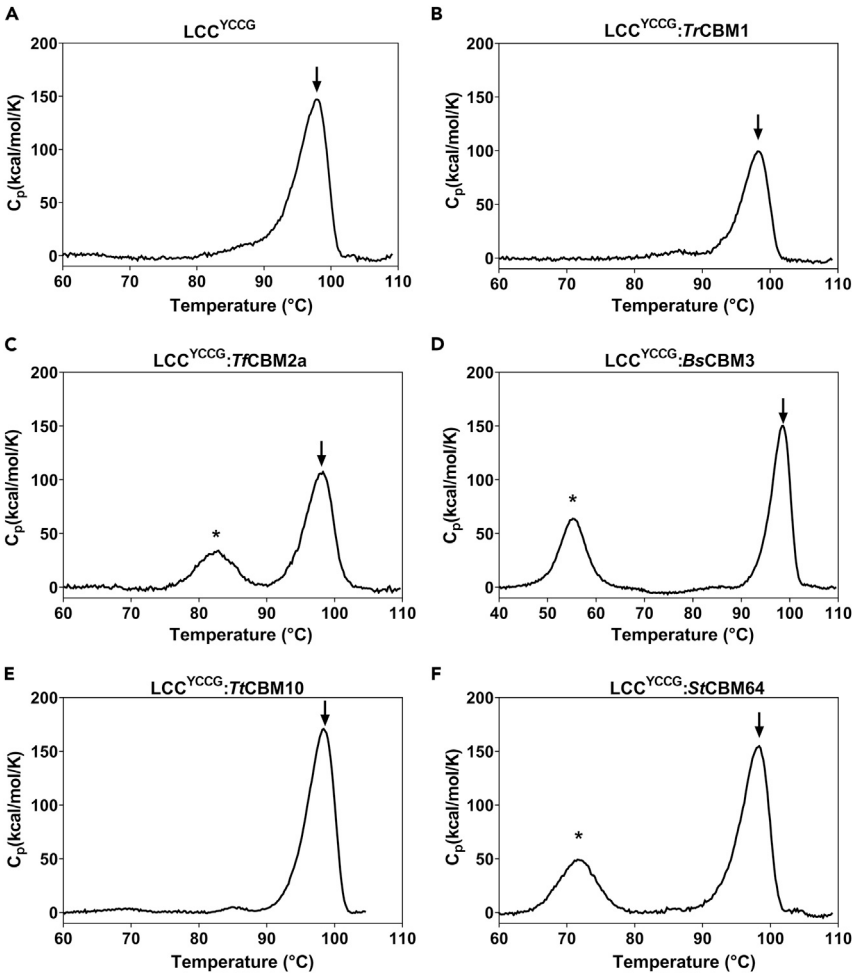

Figure 3. Thermostability of component domains in LCC^{YCCG}:CBM fusions

(A–F) Protein DSC thermograms for LCC^{YCCG} (A), LCC^{YCCG}:*Tr*CBM1 (B), LCC^{YCCG}:*Tf*CBM2a (C), LCC^{YCCG}:*Bs*CBM3 (D), LCC^{YCCG}:*Tt*CBM10 (E), and LCC^{YCCG}:*St*CBM64 (F). The arrow on each panel indicates the unfolding transition (T_m) of the LCC^{YCCG} catalytic domain, and an asterisk (*) indicates the identified CBM unfolding transition. Each analysis was performed in triplicate (Table S4). Data are available in Data S2.

Despite its enhancement of PET surface binding by LCC^{YCCG} (Figure 2B), the *Tr*CBM1 did not exhibit a detectable denaturation transition in the DSC thermograms, either as an isolated domain or in the context of the LCC^{YCCG}:*Tr*CBM1 fusion (Figure 3); the same phenomenon was observed for the LCC^{YCCG}:*Tt*CBM10 fusion.

Some fusion enzymes exhibit enhanced substrate hydrolysis at low PET loading across a range of temperatures

Amorphous PET hydrolysis activity was evaluated from 40°C to 90°C at low PET loadings (2 wt %), and a detectable yield of aromatic PET monomers was observed for all fusion enzymes (Figures 4 and S2). The highest hydrolysis activities were observed at 70°C; above this temperature, recrystallization of the amorphous PET accelerates, resulting in reduced accessibility for the active site to individual polymer substrate chains.[22] At 90°C, the further reduction in PET hydrolysis activity may reflect irreversible denaturation of the LCC^{YCCG} due to kinetic instability on approaching its apparent T_m.

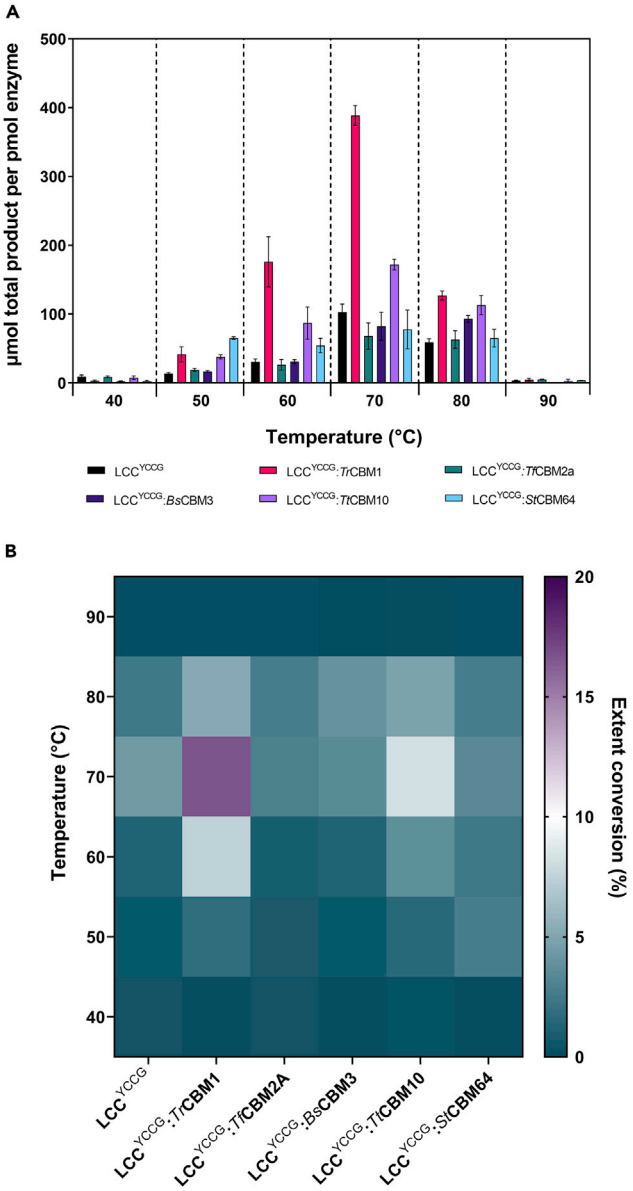

Figure 4. Temperature dependence of PET hydrolysis for LCC^{YCCG} and LCC^{YCCG}:CBM fusion enzymes at low solids loading in small-scale reactions

(A) Enzyme performance is depicted as µmol total aromatic product/pmol of enzyme following incubation for 24 h reactions at 2 wt % PET loading (equivalent to 0.13 mg enzyme/g PET for LCC^{YCCG}), reported from 30°C to 90°C for 100 nM of each fusion enzyme or the LCC^{YCCG} catalytic domain alone. Error bars represent the SD of measurements from triplicate reactions. Graphs showing the yield of each monomer product (BHET, MHET, and TPA) are presented in Figure S2.

(B) Heatmap of the extent of PET conversion calculated from the yield of monomeric aromatic products.

Data are available in Data S2.

Across the 50°C–80°C temperature range, the *Tr*CBM1 and *Tt*CBM10 fusions consistently outperform the isolated LCC^{YCCG} catalytic domain in PET hydrolysis. The *St*CBM64 fusion also exhibits enhanced activity, but only at 50°C and 60°C. These enhancements require the CBM and the catalytic domain to be covalently linked; equimolar mixtures of LCC^{YCCG} with either *Tr*CBM1 or *St*CBM64 do not stimulate

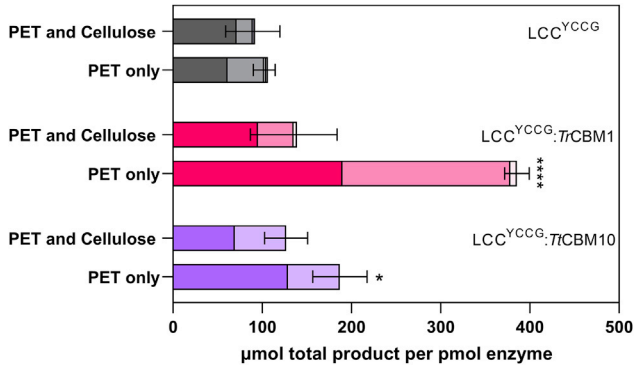

Figure 5. Cellulose binding activity of the *Tr*CBM1 and *Tt*CBM10 fusion enzymes

Cellulose binding competition assay performed at 70°C was used to ascertain whether native cellulose-binding function is present for the *Tr*CBM1 and *Tt*CBM10 fusion enzymes. Each stacked bar shows the monomeric aromatic product released for TPA (heavy shading), MHET (medium shading), and BHET (light shading). Error bars represent the SD of the total product from triplicate reactions. Statistical comparisons (*$p > 0.05$; ****$p < 0.0001$) between PET-only and PET-plus-cellulose experiments are indicated on the graph.

Data are available in Data S2.

hydrolysis (Figure S3). Furthermore, elevated concentrations of isolated CBMs do not inhibit hydrolysis—either at low or high PET loading—as would be expected if they competed with the LCC^{YCCG} for substrate binding (Figure S3).

In these small-scale, low-solids loading experiments, the highest extent of PET conversion was observed for the LCC^{YCCG}:*Tr*CBM1 fusion at 70°C; under these conditions, the yield of aromatic products was approximately 4-fold higher than that of the LCC^{YCCG} catalytic domain alone. Since the fusion enzymes have comparable BHET hydrolysis activity (Figure S1), this dramatic enhancement in PET hydrolase activity in LCC^{YCCG}:*Tr*CBM1 can be attributed to an improved enzyme-PET substrate interaction. Scanning electron microscopy (SEM) analysis of residual films following incubation with each LCC^{YCCG}:CBM fusion at 70°C reveals degraded and pitted surfaces characteristic of enzyme-mediated PET hydrolysis (Figure S4). Despite the failure of these CBMs to display a thermal unfolding transition in the DSC experiments, the *Tr*CBM1 and *Tt*CBM10 fusions clearly stimulate PET hydrolysis between 50°C and 80°C and, hence, are likely to be correctly folded within this range.

To provide further evidence that these CBMs are functionally active in associating with PET, we conducted PET hydrolysis reactions in the presence of cellulose, the natural binding partner for these CBMs, as a competitor (Figure 5). The yield of PET aromatic monomers significantly decreased in the presence of cellulose, confirming that *Tr*CBM1 and *Tt*CBM10 are indeed functionally active in the two fusion enzymes.

Screening LCC^{YCCG}:*Tr*CBM1, LCC^{YCCG}:*Tt*CBM10, and LCC^{YCCG}:*St*CBM64 at 1–20 wt % PET loading

We have established that, at 2 wt % PET loading, fusing LCC^{YCCG} with either *Tr*CBM1, *Tt*CBM10, or, to a lesser extent, *St*CBM64 can improve PET hydrolysis. Next, we investigated whether this improvement is evident at a range of PET loadings up to 20 wt %. For the *Tr*CBM1 and *Tt*CBM10 fusions, these experiments were performed at 70°C, the optimal temperature for PET hydrolysis by LCC^{YCCG}; for LCC^{YCCG}:*St*CBM64, this reaction was performed at 50°C, which is considerably below the optimal reaction temperature for LCC^{YCCG} (70°C), with the intent to

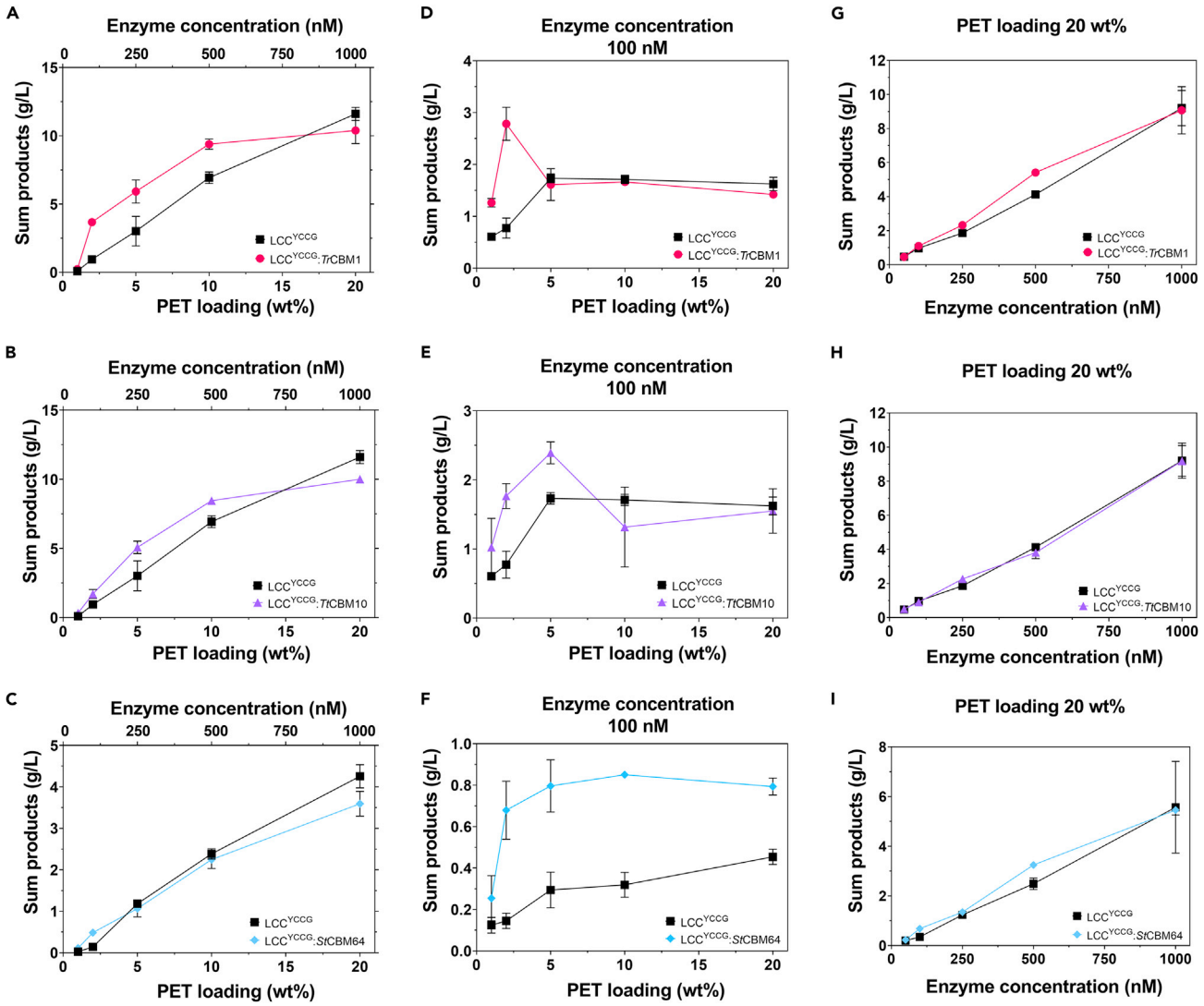

Figure 6. Comparison of PET hydrolysis by LCC^{YCCG} and LCC^{YCCG}:CBM fusion enzymes at up to 20 wt % PET loadings in small-scale reactions

(A–I) Each panel shows the sum of aromatic products (TPA, MHET, and BHET) resulting from 500 μL hydrolysis reactions at various substrate loadings (1–20 wt %), where either the enzyme:substrate ratio is maintained (corresponding to 0.13 mg LCC^{YCCG}/g PET) (A–C), the molar concentration of enzyme is held constant at 100 nM (D–F), or the substrate loading is held constant at 20 wt % (G–I).

(A, B, D, E, G, and H) Data from reactions performed at 70°C, and (C, F, and I) data from reactions at 50°C. Error bars represent the SD of measurements from triplicate reactions.

Graphs showing the yield of each monomer product are presented in Figure S6. Data are available in Data S2.

maintain the structural integrity of the *St*CBM64. None of these LCC^{YCCG}:CBM fusion enzymes shows any sign of breakdown into the individual domains under the reaction conditions employed over a 24 h period (Figure S5), confirming that in each case, the inter-domain linker is resistant to breakdown by any potentially contaminating proteases despite its lack of glycosylation.

Fusion of *Tr*CBM1, *Tt*CBM10, and *St*CBM64 to LCC^{YCCG} improves monomer yield in most reaction conditions up to 5 wt % PET loading (Figures 6 and S6). The LCC^{YCCG}:*Tr*CBM1 fusion generates the highest increase in yield at 70°C, achieving 3-fold higher monomer accumulation than LCC^{YCCG} at the optimal reaction conditions for the catalytic domain alone. (Figures 6A and 6D). The LCC^{YCCG}:*Tt*CBM10

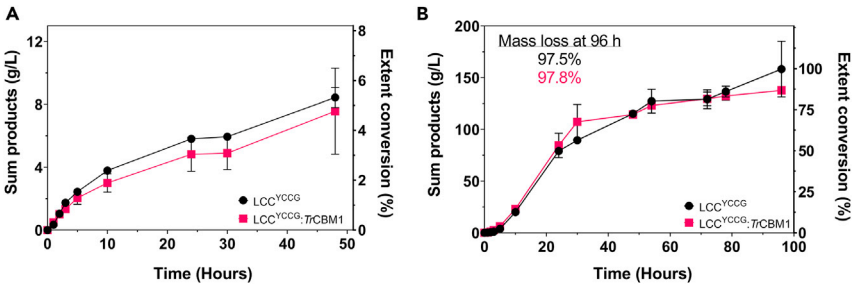

Figure 7. Time course of PET hydrolysis at high PET solids loading with continuous pH control

Each panel shows the sum of aromatic products resulting from 1 L reactions with continuous pH, agitation, and temperature control (pH 7.5, 200 RPM, 65°C). Error bars represent the range of reactions performed in duplicate. Graphs showing the yield of each aromatic monomer product are presented in Figure S8. Extent of conversion calculations are based on product yields. Data are available in Data S2.

(A) Reactions over 48 h containing 1 μM enzyme (0.13 mg LCC^{YCCG}/g PET, and 0.15 mg LCC^{YCCG}:*Tr*CBM1/g PET) and 20 wt % PET loading.

(B) Reactions over 96 h containing 12.7 μM enzyme (1.65 mg LCC^{YCCG}/g PET, 1.90 mg LCC^{YCCG}:*Tr*CBM1/g PET) at 20 wt % PET loading. Mass loss measured at end of 96 h for LCC^{YCCG} was 97.5% and for LCC^{YCCG}:*Tr*CBM1 was 97.8%.

fusion generates up to a 2-fold increase between 2–5 wt % PET loading (Figures 6B and 6E). It is noteworthy that LCC^{YCCG}:*St*CBM64 showed a 4-fold increase in monomer yield over the LCC^{YCCG} catalytic domain alone for up to 2 wt % PET loading (Figure 6C).

Above 10 wt % PET loading, fusion enzymes do not improve substrate hydrolysis

At PET loadings from 10 to 20 wt % PET, any advantage conferred by the fusion of the CBM to the LCC^{YCCG} catalytic domain at lower PET loadings was no longer observed (Figures 6 and S6). Indeed, at the highest PET loading, LCC^{YCCG} generates a higher yield of monomer products than any of the fusions. In the case of the LCC^{YCCG}:*St*CBM64, despite maintaining a 2-fold increase over the LCC^{YCCG} catalytic domain alone at 20 wt % PET loading with fixed enzyme concentration (100 nM), the overall level of PET hydrolysis under these reaction conditions (50°C) is significantly lower than what can be achieved by LCC^{YCCG} alone at its optimal reaction temperature (70°C) (Figures 6C and 6F). Furthermore, at 20 wt % PET loading, the most industrially significant level, the *Tr*CBM1, *Tt*CBM10, and *St*CBM64 fusions show no sustained advantage over the LCC^{YCCG} domain alone over the enzyme concentration range 50 nM to 1 μM (Figures 6G–6I); in each case, the aromatic monomer product yield rises approximately linearly with enzyme concentration.

To evaluate the effect of the binding module fusions under industrially relevant conditions, reactions were performed in 3 L bioreactors with 1 L reaction volume and continuous pH, agitation, and temperature control at a PET loading of 20 wt % (Figure 7). To achieve the high enzyme loading needed for these experiments, the LCC^{YCCG}:*Tr*CBM1 genetic construct was redesigned to have an N-terminal histidine tag, which increased expression yield while maintaining a similar activity profile (Figure S7). An initial trial, meant to recapitulate the small-scale experiments (those presented in Figure 6) at 20 wt % PET loading and an equivalent enzyme loading (1 μM), confirms that LCC^{YCCG}:*Tr*CBM1 does not demonstrate improved PET hydrolysis at higher PET loadings compared with the LCC^{YCCG} enzyme alone (Figures 7A, S8A, and S8B). The subsequent experiment sought to

completely hydrolyze solid PET to its monomer products. Using 20 wt % PET loading (200 g/L) and a higher enzyme loading (12.7 μM), approximately 97% measured mass loss was achieved over the 96 h reaction time for both LCC^{YCCG} and LCC^{YCCG}:*Tr*CBM1 reactions, with no significant difference in the product accumulation profile observed over the entire reaction time course (Figure 7B, S8C, and S8D).

DISCUSSION

The efficiency of enzymatic PET hydrolysis is dependent on the enzyme-substrate interaction. To explore the effect of coupling an accessory binding domain and a PET hydrolase, we analyzed fusion enzymes pairing a CBM from five different CBM families (1, 2a, 3, 10, and 64) to the highly active LCC^{YCCG} enzyme variant. We demonstrate that all LCC^{YCCG} fusions tested are functionally active on PET. The most active fusion enzymes pair with CBMs from families 1 and 10; these small CBMs (approximately 36 and 50 residues, respectively) are suggested to have a flexible fold susceptible to secondary and tertiary structural changes,[49] with flexible loop regions.[33,34,49–52]

In agreement with previous studies on fusions of binding domains with PET hydrolases, at low substrate loadings (<3 wt % PET), LCC^{YCCG}:*Tr*CBM1 and LCC^{YCCG}:*Tt*CBM10 exhibited significantly higher product yields than the LCC^{YCCG} catalytic domain alone. However, as the wt % PET loading is increased, with either the same enzyme:PET loading (equivalent to 0.13 mg LCC^{YCCG}/g PET) or a constant enzyme concentration (100 nM), the LCC^{YCCG}:*Tr*CBM1 and LCC^{YCCG}:*Tt*CBM10 fusion enzymes lose any advantage, and by 20 wt % PET loading, it is completely lost. Therefore, any advantage of the synthetic fusion constructs is realized only at low-solids loadings. This is consistent with previous findings by Varnai et al., who reported that the CBMs of cellobiohydrolases do not enhance enzymatic cellulose hydrolysis at high-solids loadings.[42] Similarly, in this study, the elevated solids loading increases the frequency of enzyme-substrate collisions and accelerates PET hydrolysis to the point where the presence of the CBM no longer provides any additional benefit.

Interestingly, for LCC^{YCCG}:*St*CBM64 at 50°C and constant enzyme concentration (100 nM), the catalytic advantage over LCC^{YCCG} is maintained across PET loadings (Figure 6F), but the temperature mismatch between *St*CBM64 thermostability and LCC^{YCCG} optimal activity limits the application of this LCC^{YCCG}:CBM fusion.

In this study, only amorphous PET film has been tested, and therefore future studies should investigate the observed behavior of CBMs for PET substrates with different physical morphologies including parameters such as crystallinity, accessible surface area, and chemical purity. Furthermore, with the continuing development of more efficient PET hydrolyses, it may be of interest to consider alternative catalytic domains, linkers, and CBMs.

Conclusions

CBMs can convey substantial advantages in PET hydrolysis at low substrate loading, namely in the range of 1–5 wt % PET. However, at the optimal reaction temperature for LCC^{YCCG} performance, the beneficial role of CBM fusions is reduced at high substrate loadings (10–20 wt % PET). This is confirmed in reactions with constant pH control and at high extents of conversion to monomeric products. Overall, for

the CBMs studied herein, we conclude there is little industrial relevance for CBM fusion enzymes above 10 wt % PET loading for amorphous PET substrates.

EXPERIMENTAL PROCEDURES

Resource availability

Lead contact

Further information and requests for resources should be directed to and will be fulfilled by the lead contact, Andrew R. Pickford (andy.pickford@port.ac.uk).

Materials availability

This study did not generate new materials. The amorphous PET film used throughout this study was supplied by Goodfellow (catalog number ES301445; 0.25 mm thickness); it was either hole punched to 10 × 13 mm for all small-scale experiments or cut into uniform pieces of approximately 0.5 × 0.5 cm for large-scale experiments.

Data and code availability

The datasets generated during this study are available as Data S2.

SUPPLEMENTAL INFORMATION

Supplemental information can be found online at https://doi.org/10.1016/j.checat.2022.07.018.

ACKNOWLEDGMENTS

We thank the members of the Bio-Optimized Technologies to Keep Thermoplastics Out of Landfills and the Environment (BOTTLE Consortium) and the Center for Enzyme Innovation for helpful discussions. We thank Mackenzie Denton for technical assistance. R.G., J.E.M., and A.R.P. were supported by Research England through the Expanding Excellence in England (E3) scheme. Funding for E.E., R.K.B., D.S., G.T.B., and J.E.M. was provided by the US Department of Energy, Office of Energy Efficiency and Renewable Energy, Advanced Manufacturing Office (AMO) and Bioenergy Technologies Office (BETO), and funding for Y.L. and Z.T. was provided by the National Key R & D Program of China (2018YFE0111400). This work was performed as part of the BOTTLE Consortium and was supported by AMO and BETO under contract no. DE-AC36-08GO28308 with the National Renewable Energy Laboratory (NREL), operated by Alliance for Sustainable Energy, LLC. The BOTTLE consortium includes members from the University of Portsmouth, funded under contract no. DE-AC36-08GO28308 with NREL. The views expressed in the article do not necessarily represent the views of the DOE or the US government. The US government retains and the publisher, by accepting the article for publication, acknowledges that the US government retains a non-exclusive, paid-up, irrevocable, worldwide license to publish or reproduce the published form of this work, or allow others to do so, for US government purposes.

AUTHOR CONTRIBUTIONS

R.G., E.E., G.T.B., J.E.M., and A.R.P. designed the study. R.G. carried out the enzyme expression, binding assays, small-scale digestion experiments, and DSC measurements. The large-scale bioreactor experiments were designed by R.G., E.E., and R.K.B. and were conducted by E.E., R.K.B., D.S., and W.E.M. CBMs for control experiments were supplied by Y.L. and Z.T. R.G., E.E., G.T.B., J.E.M., and A.R.P. conducted the data analysis. The manuscript was written by R.G., E.E., G.T.B., J.E.M., and A.R.P. and was edited and approved by all authors.

DECLARATION OF INTERESTS

The authors declare no competing interests.

Received: May 18, 2022
Revised: July 5, 2022
Accepted: July 20, 2022
Published: August 23, 2022

REFERENCES

1. Carniel, A., Waldow, V.d.A., and Castro, A.M.d. (2021). A comprehensive and critical review on key elements to implement enzymatic PET depolymerization for recycling purposes. Biotechnol. Adv. *52*, 107811. https://doi.org/10.1016/j.biotechadv.2021.107811.

2. Jambeck, J.R., Geyer, R., Wilcox, C., Siegler, T.R., Perryman, M., Andrady, A., Narayan, R., and Law, K.L. (2015). Plastic waste inputs from land into the ocean. Science *347*, 768–771. https://doi.org/10.1126/science.1260352.

3. Geyer, R., Jambeck, J.R., and Law, K.L. (2017). Production, use, and fate of all plastics ever made. Sci. Adv. *3*, e1700782. https://doi.org/10.1126/sciadv.1700782.

4. Borrelle, S.B., Ringma, J., Law, K.L., Monnahan, C.C., Lebreton, L., McGivern, A., Murphy, E., Jambeck, J., Leonard, G.H., Hilleary, M.A., et al. (2020). Predicted growth in plastic waste exceeds efforts to mitigate plastic pollution. Science *369*, 1515–1518. https://doi.org/10.1126/science.aba3656.

5. Sheldon, R.A., and Brady, D. (2022). Green chemistry, biocatalysis, and the chemical industry of the future. ChemSusChem *15*, e202102628. https://doi.org/10.1002/cssc.202102628.

6. Wei, R., and Zimmermann, W. (2017). Microbial enzymes for the recycling of recalcitrant petroleum-based plastics: how far are we? Microb. Biotechnol. *10*, 1308–1322. https://doi.org/10.1111/1751-7915.12710.

7. Wei, R., and Zimmermann, W. (2017). Biocatalysis as a green route for recycling the recalcitrant plastic polyethylene terephthalate. Microb. Biotechnol. *10*, 1302–1307. https://doi.org/10.1111/1751-7915.12714.

8. Danso, D., Chow, J., and Streit, W.R. (2019). Plastics: Environmental and biotechnological perspectives on microbial degradation. Appl. Environ. Microbiol. *85*, e01095. https://doi.org/10.1128/AEM.01095-19.

9. Wei, R., Tiso, T., Bertling, J., O'Connor, K., Blank, L.M., and Bornscheuer, U.T. (2020). Possibilities and limitations of biotechnological plastic degradation and recycling. Nat. Catal. *3*, 867–871. https://doi.org/10.1038/s41929-020-00521-w.

10. Martín, A.J., Mondelli, C., Jaydev, S.D., and Pérez-Ramírez, J. (2021). Catalytic processing of plastic waste on the rise. Chem *7*, 1487–1533. https://doi.org/10.1016/j.chempr.2020.12.006.

11. Ellis, L.D., Rorrer, N.A., Sullivan, K.P., Otto, M., McGeehan, J.E., Román-Leshkov, Y., Wierckx, N., and Beckham, G.T. (2021). Chemical and biological catalysis for plastics recycling and upcycling. Nat. Catal. *4*, 539–556. https://doi.org/10.1038/s41929-021-00648-4.

12. Wei, R., von Haugwitz, G., Pfaff, L., Mican, J., Badenhorst, C.P.S., Liu, W., Weber, G., Austin, H.P., Bednar, D., Damborsky, J., and Bornscheuer, U.T. (2022). Mechanism-based design of efficient PET hydrolases. ACS Catal. *12*, 3382–3396. https://doi.org/10.1021/acscatal.1c05856.

13. Taniguchi, I., Yoshida, S., Hiraga, K., Miyamoto, K., Kimura, Y., and Oda, K. (2019). Biodegradation of PET: current status and application aspects. ACS Catal. *9*, 4089–4105. https://doi.org/10.1021/acscatal.8b05171.

14. Kawai, F., Kawabata, T., and Oda, M. (2020). Current state and perspectives related to the Polyethylene Terephthalate hydrolases available for biorecycling. ACS Sustain. Chem. Eng. *8*, 8894–8908. https://doi.org/10.1021/acssuschemeng.0c01638.

15. Herrero Acero, E., Ribitsch, D., Dellacher, A., Zitzenbacher, S., Marold, A., Steinkellner, G., Gruber, K., Schwab, H., and Guebitz, G.M. (2013). Surface engineering of a cutinase from *Thermobifida Cellulosilytica* for improved polyester hydrolysis. Biotechnol. Bioeng. *110*, 2581–2590. https://doi.org/10.1002/bit.24930.

16. Kawai, F., Oda, M., Tamashiro, T., Waku, T., Tanaka, N., Yamamoto, M., Mizushima, H., Miyakawa, T., and Tanokura, M. (2014). A novel Ca2+-activated, thermostabilized polyesterase capable of hydrolyzing polyethylene terephthalate from *Saccharomonospora viridis* AHK190. Appl. Microbiol. Biotechnol. *98*, 10053–10064. https://doi.org/10.1007/s00253-014-5860-y.

17. Furukawa, M., Kawakami, N., Oda, K., and Miyamoto, K. (2018). Acceleration of enzymatic degradation of Poly(ethylene terephthalate) by surface coating with anionic surfactants. ChemSusChem *11*, 4018–4025. https://doi.org/10.1002/cssc.201802096.

18. Oda, M., Yamagami, Y., Inaba, S., Oida, T., Yamamoto, M., Kitajima, S., and Kawai, F. (2018). Enzymatic hydrolysis of PET: functional roles of three Ca2+ ions bound to a cutinase-like enzyme, Cut190*, and its engineering for improved activity. Appl. Microbiol. Biotechnol. *102*, 10067–10077. https://doi.org/10.1007/s00253-018-9374-x.

19. Austin, H.P., Allen, M.D., Donohoe, B.S., Rorrer, N.A., Kearns, F.L., Silveira, R.L., Pollard, B.C., Dominick, G., Duman, R., El Omari, K., et al. (2018). Characterization and engineering of a plastic-degrading aromatic polyesterase. Proc. Natl. Acad. Sci. USA *115*, E4350–E4357. https://doi.org/10.1073/pnas.1718804115.

20. Joo, S., Cho, I.J., Seo, H., Son, H.F., Sagong, H.Y., Shin, T.J., Choi, S.Y., Lee, S.Y., and Kim, K.J. (2018). Structural insight into molecular mechanism of poly(ethylene terephthalate) degradation. Nat. Commun. *9*, 382. https://doi.org/10.1038/s41467-018-02881-1.

21. Son, H.F., Cho, I.J., Joo, S., Seo, H., Sagong, H.Y., Choi, S.Y., Lee, S.Y., and Kim, K.J. (2019). Rational protein engineering of thermo-stable PETase from *Ideonella sakaiensis* for highly efficient PET degradation. ACS Catal. *9*, 3519–3526. https://doi.org/10.1021/acscatal.9b00568.

22. Tournier, V., Topham, C.M., Gilles, A., David, B., Folgoas, C., Moya-Leclair, E., Kamionka, E., Desrousseaux, M.L., Texier, H., Gavalda, S., et al. (2020). An engineered PET depolymerase to break down and recycle plastic bottles. Nature *580*, 216–219. https://doi.org/10.1038/s41586-020-2149-4.

23. Cui, Y., Chen, Y., Liu, X., Dong, S., Tian, Y., Qiao, Y., Mitra, R., Han, J., Li, C., Han, X., et al. (2021). Computational redesign of a PETase for plastic biodegradation under ambient condition by the GRAPE strategy. ACS Catal. *11*, 1340–1350. https://doi.org/10.1021/acscatal.0c05126.

24. Espino-Rammer, L., Ribitsch, D., Przylucka, A., Marold, A., Greimel, K.J., Herrero Acero, E., Guebitz, G.M., Kubicek, C.P., and Druzhinina, I.S. (2013). Two novel class ii hydrophobins from *Trichoderma spp.* Stimulate enzymatic hydrolysis of poly(ethylene terephthalate) when expressed as fusion proteins. Appl. Environ. Microbiol. *79*, 4230–4238. https://doi.org/10.1128/AEM.01132-13.

25. Ribitsch, D., Yebra, A.O., Zitzenbacher, S., Wu, J., Nowitsch, S., Steinkellner, G., Greimel, K., Doliska, A., Oberdorfer, G., Gruber, C.C., et al. (2013). Fusion of binding domains to *Thermobifida cellulosilytica* cutinase to tune sorption characteristics and enhancing PET hydrolysis. Biomacromolecules *14*, 1769–1776. https://doi.org/10.1021/bm400140u.

26. Ribitsch, D., Herrero Acero, E., Przylucka, A., Zitzenbacher, S., Marold, A., Gamerith, C., Tscheließnig, R., Jungbauer, A., Rennhofer, H., Lichtenegger, H., et al. (2015). Enhanced cutinase-catalyzed hydrolysis of polyethylene terephthalate by covalent fusion to hydrophobins. Appl. Environ. Microbiol. *81*, 3586–3592. https://doi.org/10.1128/AEM.04111-14.

27. Puspitasari, N., Tsai, S.L., and Lee, C.K. (2021). Fungal hydrophobin RolA enhanced PETase hydrolysis of polyethylene terephthalate. Appl. Biochem. Biotechnol. *193*, 1284–1295. https://doi.org/10.1007/s12010-020-03358-y.

28. Dai, L., Qu, Y., Huang, J.-W., Hu, Y., Hu, H., Li, S., Chen, C.-C., and Guo, R.-T. (2021). Enhancing PET hydrolytic enzyme activity by fusion of the cellulose–binding domain of cellobiohydrolase I from *Trichoderma reesei*. J. Biotechnol. *334*, 47–50. https://doi.org/10.1016/j.jbiotec.2021.05.006.

29. Xue, R., Chen, Y., Rong, H., Wei, R., Cui, Z., Zhou, J., Dong, W., and Jiang, M. (2021). Fusion of chitin-binding domain from *Chitinolyticbacter meiyuanensis* SYBC-H1 to the Leaf-branch compost cutinase for enhanced PET hydrolysis. Front. Bioeng. Biotechnol. *9*, 762854. https://doi.org/10.3389/fbioe.2021.762854.

30. Vaaje-Kolstad, G., Westereng, B., Horn, S.J., Liu, Z., Zhai, H., Sørlie, M., and Eijsink, V.G.H. (2010). An oxidative enzyme boosting the enzymatic conversion of recalcitrant polysaccharides. Science *330*, 219–222. https://doi.org/10.1126/science.1192231.

31. Gilbert, H.J., Knox, J.P., and Boraston, A.B. (2013). Advances in understanding the molecular basis of plant cell wall polysaccharide recognition by carbohydrate-binding modules. Curr. Opin. Struct. Biol. *23*, 669–677. https://doi.org/10.1016/j.sbi.2013.05.005.

32. Payne, C.M., Knott, B.C., Mayes, H.B., Hansson, H., Himmel, M.E., Sandgren, M., Ståhlberg, J., and Beckham, G.T. (2015). Fungal cellulases. Chem. Rev. *115*, 1308–1448. https://doi.org/10.1021/cr500351c.

33. Kraulis, J., Clore, G.M., Nilges, M., Jones, T.A., Pettersson, G., Knowles, J., and Gronenborn, A.M. (1989). Determination of the three-dimensional solution structure of the C-terminal domain of Cellobiohydrolase I from *Trichoderma reesei* . A study using nuclear magnetic resonance and hybrid distance geometry-dynamical simulated annealing. Biochemistry *28*, 7241–7257. https://doi.org/10.1021/BI00444A016.

34. Beckham, G.T., Matthews, J.F., Bomble, Y.J., Bu, L., Adney, W.S., Himmel, M.E., Nimlos, M.R., and Crowley, M.F. (2010). Identification of amino acids responsible for processivity in a family 1 carbohydrate-binding module from a fungal cellulase. J. Phys. Chem. B *114*, 1447–1453. https://doi.org/10.1021/jp908810a.

35. Nishiyama, Y., Langan, P., and Chanzy, H. (2002). Crystal structure and hydrogen-bonding system in cellulose Iβ from synchrotron X-ray and neutron fiber diffraction. J. Am. Chem. Soc. *124*, 9074–9082. https://doi.org/10.1021/ja0257319.

36. Nishiyama, Y., Sugiyama, J., Chanzy, H., and Langan, P. (2003). Crystal structure and hydrogen bonding system in cellulose Iα from synchrotron X-ray and neutron fiber diffraction. J. Am. Chem. Soc. *125*, 14300–14306. https://doi.org/10.1021/ja037055w.

37. Gamerith, C., Herrero Acero, E., Pellis, A., Ortner, A., Vielnascher, R., Luschnig, D., Zartl, B., Haernvall, K., Zitzenbacher, S., Strohmeier, G., et al. (2016). Improving enzymatic polyurethane hydrolysis by tuning enzyme sorption. Polym. Degrad. Stab. *132*, 69–77. https://doi.org/10.1016/j.polymdegradstab.2016.02.025.

38. Liu, Z., Zhang, Y., and Wu, J. (2022). Enhancement of PET biodegradation by anchor peptide-cutinase fusion protein. Enzyme Microb. Technol. *156*, 110004. https://doi.org/10.1016/j.enzmictec.2022.110004.

39. Singh, A., Rorrer, N.A., Nicholson, S.R., Erickson, E., DesVeaux, J.S., Avelino, A.F., Lamers, P., Bhatt, A., Zhang, Y., Avery, G., et al. (2021). Techno-economic, life-cycle, and socioeconomic impact analysis of enzymatic recycling of poly(ethylene terephthalate). Joule *5*, 2479–2503. https://doi.org/10.1016/j.joule.2021.06.015.

40. Modenbach, A.A., and Nokes, S.E. (2013). Enzymatic hydrolysis of biomass at high-solids loadings – a review. Biomass Bioenergy *56*, 526–544. https://doi.org/10.1016/j.biombioe.2013.05.031.

41. Le Costaouëc, T., Pakarinen, A., Várnai, A., Puranen, T., and Viikari, L. (2013). The role of carbohydrate binding module (CBM) at high substrate consistency: Comparison of *Trichoderma reesei* and *Thermoascus aurantiacus* Cel7A (CBHI) and Cel5A (EGII). Bioresour. Technol. *143*, 196–203. https://doi.org/10.1016/j.biortech.2013.05.079.

42. Várnai, A., Siika-aho, M., and Viikari, L. (2013). Carbohydrate-binding modules (CBMs) revisited: reduced amount of water counterbalances the need for CBMs. Biotechnol. Biofuels *6*, 30–31. https://doi.org/10.1186/1754-6834-6-30.

43. Pires, V.M.R., Pereira, P.M.M., Brás, J.L.A., Correia, M., Cardoso, V., Bule, P., Alves, V.D., Najmudin, S., Venditto, I., Ferreira, L.M.A., et al. (2017). Stability and ligand promiscuity of type A carbohydrate-binding modules are illustrated by the structure of *Spirochaeta thermophila* StCBM64C. J. Biol. Chem. *292*, 4847–4860. https://doi.org/10.1074/jbc.M116.767541.

44. Beckham, G.T., Bomble, Y.J., Matthews, J.F., Taylor, C.B., Resch, M.G., Yarbrough, J.M., Decker, S.R., Bu, L., Zhao, X., McCabe, C., et al. (2010). The O-glycosylated linker from the *Trichoderma reesei* family 7 cellulase is a flexible, disordered protein. Biophys. J. *99*, 3773–3781. https://doi.org/10.1016/j.bpj.2010.10.032.

45. Harrison, M.J., Nouwens, A.S., Jardine, D.R., Zachara, N.E., Gooley, A.A., Nevalainen, H., and Packer, N.H. (1998). Moditied glycosylation of cellobiohydrolase I from a high cellulase-producing mutant strain of *Trichoderma reesei*. Eur. J. Biochem. *256*, 119–127. https://doi.org/10.1046/j.1432-1327.1998.2560119.x.

46. Amore, A., Knott, B.C., Supekar, N.T., Shajahan, A., Azadi, P., Zhao, P., Wells, L., Linger, J.G., Hobdey, S.E., Vander Wall, T.A., et al. (2017). Distinct roles of N- and O-glycans in cellulase activity and stability. Proc. Natl. Acad. Sci. USA *114*, 13667–13672. https://doi.org/10.1073/pnas.1714249114.

47. Kari, J., Olsen, J., Borch, K., Cruys-Bagger, N., Jensen, K., and Westh, P. (2014). Kinetics of cellobiohydrolase (Cel7A) variants with lowered substrate affinity. J. Biol. Chem. *289*, 32459–32468. https://doi.org/10.1074/JBC.M114.604264.

48. Zoungrana, T., Findenegg, G.H., and Norde, W. (1997). Structure, stability, and activity of absorbed enzymes. J. Colloid Interface Sci. *190*, 437–448. https://doi.org/10.1006/jcis.1997.4895.

49. Weber, J., Petrović, D., Strodel, B., Smits, S.H.J., Kolkenbrock, S., Leggewie, C., and Jaeger, K.E. (2019). Interaction of carbohydrate-binding modules with poly(ethylene terephthalate). Appl. Microbiol. Biotechnol. *103*, 4801–4812. https://doi.org/10.1007/s00253-019-09760-9.

50. Boraston, A.B., Bolam, D.N., Gilbert, H.J., and Davies, G.J. (2004). Carbohydrate-binding modules: fine-tuning polysaccharide recognition. Biochem. J. *382*, 769–781. https://doi.org/10.1042/BJ20040892.

51. Guillén, D., Sánchez, S., and Rodríguez-Sanoja, R. (2010). Carbohydrate-binding domains: Multiplicity of biological roles. Appl. Microbiol. Biotechnol. *85*, 1241–1249. https://doi.org/10.1007/s00253-009-2331-y.

52. Taylor, C.B., Talib, M.F., McCabe, C., Bu, L., Adney, W.S., Himmel, M.E., Crowley, M.F., and Beckham, G.T. (2012). Computational investigation of glycosylation effects on a family 1 carbohydrate-binding module. J. Biol. Chem. *287*, 3147–3155. https://doi.org/10.1074/jbc.M111.270389.